Downsizing of robust Fe-triazole@SiO_2 spin-crossover nanoparticles with ultrathin shells

R. Torres-Cavanillas[1], L. Lima-Moya[1], F. D. Tichelaar[2], H.W. Zandbergen[2], M. Giménez-Marqués,[1,*] E. Coronado[1,*]

[1]*Instituto de Ciencia Molecular, Universidad de Valencia, Catedrático José Beltrán 2, 46980 Paterna, Spain.*
[2]*Kavli Institute of Nanoscience, Delft University of Technology, Lorentzweg 1, 2628 CJ Delft, The Netherlands*

A chemical protocol to design robust hybrid [Fe(Htrz)$_2$(trz)](BF$_4$)@SiO_2 nanoparticles (NPs) with sizes as small as 28 nm and ultrathin silica shells below 3 nm has been developed. These NPs present a characteristic abrupt spin transition with a subsequent decrease in the width of the thermal hysteresis upon reducing the NP size.

Spin-crossover (SCO) compounds represent a current focus of interest in Molecular Magnetism owing to their ability to undergo low-spin (LS) to high-spin (HS) transitions under the influence of external stimuli such as temperature, pressure, light or electric field.[1,2,3] In contrast to the vast majority of magnetic molecular materials, these smart materials often exhibit the spin transition near room temperature. Such a feature makes them appealing for the design of switchable devices for information processing.[4] In this context, the 1D triazole-based Fe^{II} coordination polymers of general formula [Fe(Rtrz)$_3$]X_2[5] (Rtrz = 4-R-1,2,4-triazole and X = monovalent anion) are generally considered the most promising SCO materials, since they exhibit a large thermal hysteresis near room temperature.[6]

A significant advance in this field was the miniaturization of these SCO materials in the form of nanoparticles (NPs),[7–14] promoting their use as active elements in nanoelectronic memory devices with spin-state switching functionality.[15–20] Albeit the studied SCO devices have contributed to bridge the existing gap for real application, several drawbacks still need to be solved. In particular, most of the SCO-based devices confront fatigue issues associated with their poor chemical stability[4,18], whereas the intrinsic insulating character of these SCO nanomaterials difficult practical operations.[21–23]

A way to improve the chemical robustness of the SCO NPs consists on protecting them with an inorganic silica (SiO_2) shell. This method was first used by Mallah and co-workers to synthesize SCO [Fe(pyrazine)Pt(CN)$_4$] NPs covered by silica[25] and then extended by Herrera, Colacio and co-workers to wrap the triazole-based coordination polymer [Fe(Htrz)$_2$(trz)](BF$_4$) with the silica shell.[26] These authors used a reverse-micelle procedure to prepare core-shell [Fe(Htrz)$_2$(trz)](BF$_4$)@SiO_2 NPs of *ca.* 100 nm presenting a thick SiO_2 shell of *ca.* 11 nm. A further variation in the synthetic protocol allowed them to reduce the particle size down to 60 nm.[27] These hybrid NPs exhibited improved chemical stability and dispersibility in different solvents, as compared to the bare SCO NPs. In addition, the SiO_2 coating provided an ideal platform for chemical functionalization via post-synthetic methods, opening a convenient way to obtain multifunctional NPs. For instance, luminescence or plasmonic properties can be incorporated in these SCO NPs by functionalizing the SiO_2 shell with luminescent molecules or gold (Au) NPs, respectively.[28–30]

Despite these attractive features, the presence of a thick SiO_2 shell has a negative effect on the performance of an electronic device based on these switching NPs. In particular, this insulating shell seriously limits the conductivity through the NPs, making difficult the detection of the spin transition since the switching occurs at very low conductivity levels.[19] To overcome this problem, the synthesis of SCO NPs protected with a thinner SiO_2 shell is mandatory. Thus, this thin shell should be sufficient to enhance the chemical stability of the pristine material, without interfering in the transport properties of the device. Furthermore, the reduced size of the NPs should facilitate even more the electrical transport. In the present work, we report the

synthesis of chemically stable Fe-triazole@SiO_2 hybrid NPs presenting different sizes (from *ca*. 90 to 28 nm) and a very thin silica shell (< 3 nm).

The general reverse-micelle procedure previously developed to cover SCO NPs with a silica shell consisted of mixing two micro-emulsions, one containing the Fe salt and the other the triazole ligand. Each one of these micro-emulsions consisted in an organic phase, formed with a non-ionic surfactant (Triton X-100), a co-surfactant (*n*-hexanol) and a hydrocarbon (cyclohexane), with an aqueous phase containing the silica precursor (tetraethyl orthosilicate, TEOS) and the Fe salt or the triazole ligand. In a second step this mixure was left to react at room temperature. In order to reduce the thickness of this silica shell, our approach consisted in adding the silica precursor (TEOS) in the organic phase, instead of adding it directly in the aqueous phase (see experimental section, SI). We assume that this modification decreases the kinetics of the hydrolysis of the hydrophilic TEOS molecules, which need first to migrate from the organic phase into the aqueous droplets of the micelles, thus resulting in a reduced growth of the silica shell.

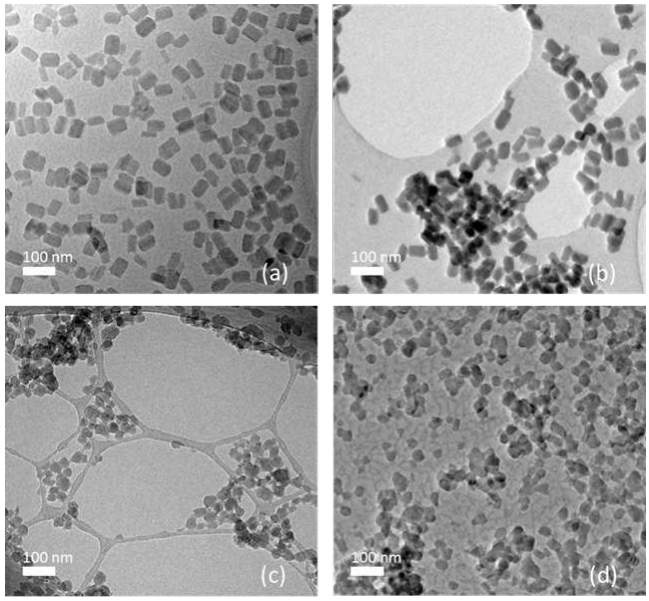

Figure 1. HR-TEM images of NPs **1** (a), **2** (b), **3** (c) and **4** (d), deposited by drop casting on holey carbon film in (a) and (c), whereas a lacey carbon film was used in (b) and (c).

In order to reduce the size of the SCO core we have acted on the key parameters involved in the NP nucleation,[10,24] namely the reaction time, the surfactant to water ratio (*i.e.* the ω parameter) and the concentration of Fe(II). Table 1 summarizes how these parameters control the size of the hybrid NPs. As we can notice, two different synthetic scenarios were required: *i)* by decreasing reaction time and Fe concentration, a size in the range 90-60 nm was obtained (**1** and **2**); *ii)* by decreasing the ratio between surfactant and water (from ω = 9 to 5) and keeping short reaction times and high Fe concentration, a reduction in the NP size down to a minimum value of 25 nm was achieved (**3** and **4**). It is important to note that attempts of using ω < 5 resulted in unstable micellar suspensions. The above results could be understood as follows: by increasing the metal concentration in the aqueous phase, the number of nucleation centers increases, leading to a decrease of the NPs final size that can further be reduced by limiting the reaction time during the micellar exchange. On the other hand, a decrease in the ω parameter results in the reduction of the micelle diameter, thus limiting the size of the NP.

Table 1. Correlation between synthetic parameters and the particle size and composition in $[Fe(Htrz)_2(trz)](BF_4)@SiO_2$ NPs.

Sample	$[Fe^{2+}]$ (M)	ω	Time (h)	Length (nm)	Width (nm)	Si/Fe
1	1.25	9	24	87 ± 8	49 ± 13	0.7
2	1.5	9	2	60 ± 8	39 ± 8	0.8
3	1.5	8	2	38 ± 7	-	0.8
4	1.5	5	2	28 ± 6	-	1.1

The stability of these hybrid $[Fe(Htrz)_2(trz)](BF_4)@SiO_2$ NPs has been proved from Dynamic Light Scattering measurements in colloidal aqueous suspensions. Essentially, dried samples of NPs **1**-**4** can be re-dispersed in different solvents including water, maintaining their colloidal and chemical stability up to 3 days. This observation is in sharp contrast with what happens in the pure $[Fe(Htrz)_2(trz)](BF_4)$ NPs coated with organic AOT (AOT = dioctyl sulfosuccinate sodium salt), which are not redispersable once dried in any solvent and rapidly degrade in the form of oxidized species (see Figure S2). Therefore, the improved colloidal and chemical stability in the hybrid core@shell NPs is likely provided by the silica shell. DLS measurements performed in these colloidal suspensions afforded hydrodynamic diameter of 137 ± 8 and 68 ± 9 nm for NPs **1** and **2,** and 47 ± 8 and 29 ± 9 nm for NPs **3** and **4** (Figure S1). These values are consistent with the more precise values observed by High-Resolution Transmission Electron Microscopy (HR-TEM), which in addition also give information on the morphology and composition of the hybrid NPs. NPs **1-2** present a rod-like morphology with an average side length of 87 ± 8 and 60 ± 8 nm respectively, whereas NPs **3**-**4** tend to be spherical with a diameter of 38 ± 7 and 28 ± 6 nm, respectively (see Table 1).

To establish the presence of Si and Fe in the NPs, energy-dispersive X-ray spectroscopy (EDS) experiments were performed. Several NPs were mapped for samples **1**, **3** and **4** for statistical purposes. In all cases, the presence of O and Si was clearly evidenced (see Figure 2 and S5). However, the determination of the shell thickness resulted more challenging due to a persistent contamination related to the detection limit of the microscope and the shell thickness (close to 1 nm). Only in the case of NPs **1** presenting the largest size, a sharp oxygen shell of *ca.* 3 nm was observed (see Figure 2a). In the smaller hybrid NPs (samples **2**, **3** and **4**) the silica shell was indistinguishable from the core.

To proof the presence of a silica coverage in the smallest NPs (sample **4**), we used a chemical approach developed by Li and co-workers[30] which consists in decorating the silica shell with Au NPs. The Au decoration protocol consisted in the post- functionalization of the silica shell with (3-aminopropyl)triethoxysilane (APTES) to form **4@NH₂** NPs. These amino-functionalized NPs were then decorated with $HAuCl_4$ molecules taking advantage of the electrostatic interactions between the $AuCl_4^-$ anions and the amino terminal groups. Finally, the anchored anions were reduced *in situ* to form **4@Au** NPs. It is important to note that the original work of Li and co-workers used large SCO NPs of *ca*. 200 nm, whereas in this case the chemical Au decoration is achieved using NPs of *ca.* 28 nm. HR-TEM image represented in Figure 2b reveals the successful decoration

of the core-shell NPs **4** with Au NPs of *ca.* 4 nm with a high degree of grafting. Such a directed surface chemistry unequivocally evidences the presence of a thin silica shell and results unsuccessful when pristine SCO NPs are used instead.

Figure 2. (a) Annular Dark Field (ADF) STEM image of NPs **1** and EDS maps of Fe and O. (b)TEM image of NPs **4** decorated with Au nanoparticles.

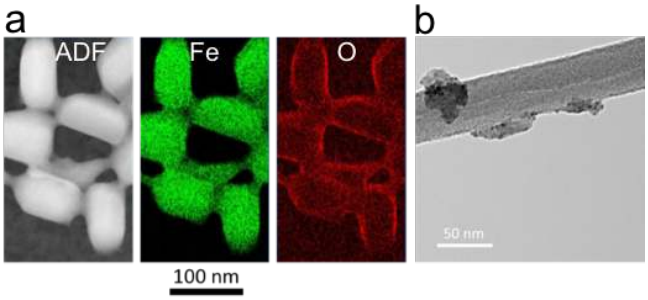

The structure and composition of the $[Fe(Htrz)_2(trz)](BF_4)$ @SiO_2 hybrid NPs were established by X-ray powder diffraction and inductively coupled plasma optical emission spectrometry (ICP-OES). X-ray powder diffraction of the hybrid NPs **1**-**4** revealed the existence of one single phase corresponding to the simulated pattern of $[Fe(Htrz)_2(trz)](BF_4)$ coordination polymer (see Figure S3).[32,33] ICP-OES was used to quantify the amount of Si and Fe after digestion of the NPs under acidic conditions. A molar ratio of Si/Fe comprised between 0.7 and 1.1 was obtained for NPs **1**-**4**, which results in a two times decrease of Si with respect to the already reported NPs (see Table 1).[27]

Magnetic properties of the Fe-triazole@SiO_2 hybrid NPs were studied in detail. Figure 3 shows the thermal dependence of the magnetic susceptibility times temperature ($\chi_M T$) for NPs **1**-**4**, where χ_M is the molar magnetic susceptibility in emu·mol^{-1}·K. Thermal spin transitions are characterized by the hysteresis width (ΔT) and the corresponding transition temperatures $T^{\uparrow}_{1/2}$ and $T^{\downarrow}_{1/2}$, which are defined as the temperatures for which 50% of both, the LS and HS Fe^{2+} centers are present in the sample for the heating and cooling modes, respectively. All these parameters are summarized in Table 2. $T_{1/2}$ are estimated from the maxima of the $d(\chi_M T)/dT$ curve.

Table 2. Physical parameters of the thermally induced spin transition for $[Fe(Htrz)_2(trz)](BF_4)$@SiO_2 NPs (**1**-**4**).

Sample	$T^{\uparrow}_{1/2}$ (K)	$T^{\downarrow}_{1/2}$ (K)	ΔT	HS (%)
1	376	339	37	19
2	373	344	29	18
3	366	342	24	25
4	364	342	22	41

All samples exhibit a characteristic abrupt spin transition centred above room temperature. A subsequent decrease of hysteresis width is observed upon size reduction. A 40% narrowing of the thermal hysteresis is observed, from *ca*. 40 K in NPs **1** ($T^{\uparrow}_{1/2}$ = 376 K and $T^{\downarrow}_{1/2}$ = 339 K) to *ca.* 20 K in NPs **4** ($T^{\uparrow}_{1/2}$ = 364 K and $T^{\downarrow}_{1/2}$ = 342 K). Such a thermal hysteresis decrease occurring upon size reduction may be related with a drop of the cooperativity in the material. This trend is analogous to that observed by some of us in the organic-coated SCO@AOT NPs of the same SCO material.[10] However, it is interesting to note here that similar hysteresis narrowing (*ca*. 40 %) occurs at very distinct sizes depending on the surface agent used (between *ca*. 20 and 4 nm in organic-coated NPs vs *ca*. 90 and 25 nm in inorganic-coated NPs). Essentially, such a different correlation between sizes and reduction of thermal hysteresis may be attributed to the different shell

constraint occurring in both the AOT- and SiO_2-coated NPs. The HS fraction of the NPs (between 20-40 %) is much higher than that found in bulk (*ca.* 10 %) and increases as the size of the NPs decreases as expected for the increased ratio of terminal Fe^{II} ions at the surface, which are known to remain in the HS state.

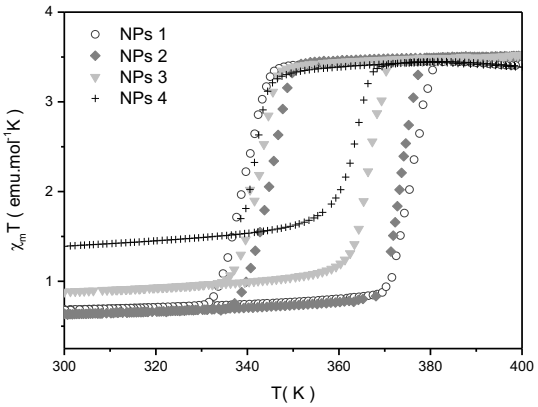

Figure 3. Comparison of the thermal variation of the $\chi_M T$ product for the different hybrid $[Fe(Htrz)_2(trz)](BF_4)@SiO_2$ NPs **1**-**4** after several heating–cooling modes.

In summary, we have synthesized a family of hybrid $[Fe(Htrz)_2(trz)](BF_4)@SiO_2$ NPs with distinct sizes (from 90 to 28 nm) using an adjusted protocol based on the reverse-micelle technique. In all cases, these SCO NPs are coated by a very thin silica shell (< 3nm), which provides colloidal and chemical stability to the NPs while enabling further surface functionalization. The size effect on the spin transition has been studied revealing the preservation of the characteristic abruptness in the spin switching accompanied by a significant decrease of the hysteresis width upon size reduction, as expected. Remarkably, a large hysteresis of *ca.* 22 K has been preserved even for the smallest NPs (*ca*. 28 nm) supporting the strong cooperativity that characterize this family of low-dimensional SCO coordination polymers.

Acknowledgments

We acknowledge funding from the EU (COST Action MOLSPIN CA15128, ERC Advanced Grant Mol-2D 788222, and RIA action COSMICS 766726), the Spanish MINECO (MAT2017-89993-R) and the Generalitat Valenciana (Prometeo Programme). R.T.-C. and M.G.-M. thank the Spanish MINECO for the FPI and Juan de la Cierva Incorporation fellowships, respectively. LCF/BQ/PI19/11690022. These results have been partly generated with the support of ”La Caixa” (ID 100010434) Fellowship LCF/BQ/PI19/11690022. Authors thank the EU support for access to the National Centre for High-Resolution Electron Microscopy in Delft (EC Grant Agreement 312483 - ESTEEM2).

Conflicts of interest

The authors declare no conflict of interest.

Notes and references

1 P. Gütlich and H. A. Goodwin, *Spin Crossover in Transition Metal Compounds I*, 2004, **1**, 1.

2 O. Kahn, J. Kröber and C. Jay Martinez, *Adv. Mater.*, 1992, **4**, 718.

3 J. F. Létard, P. Guionneau and L. Goux-Capes, *Spin Crossover Transit. Met. Compd. III*, 2004, **1**, 221.

4 O. Kahn and C. Jay Martinez, *Science* , 1998, **279**, 44.

5 L. G. Lavrenova, E. V Kirillova, V. N. Ikorskii, Y. G. Shvedenkov, V. A. Varnek, L. A. Sheludyakova and S. V Larionov, *Russian Journal of Coordination Chemistry,* 2001, **27**, 46.

6 O. Roubeau, *Chem. - A Eur. J.*, 2012, **18**, 15230.

7 E. Coronado, J. R. Galán-Mascarós, M. Monrabal-Capilla, J. García-Martínez and P. Pardo-Ibáñez, *Adv. Mater.*, 2007, **19**, 1359.

8 T. Forestier, A. Kaiba, S. Pechev, D. Denux, P. Guionneau, C. Etrillard, N. Daro, E. Freysz and J. F. Létard, *Chem. - A Eur. J.*, 2009, **15**, 6122.

9 J. R. Galán-Mascarós, E. Coronado, A. Forment-Aliaga, M. Monrabal-Capilla, E. Pinilla-Cienfuegos and M. Ceolin, *Inorg. Chem.*, 2010, **49**, 5706.

10 M. Giménez-Marqués, M. L. García-Sanz de Larrea and E. Coronado, *J. Mater. Chem. C*, 2015, **3**, 7946.

11 F. Volatron, L. Catala, E. Rivière, A. Gloter, O. Stéphan and T. Mallah, *Inorg. Chem.*, 2008, **47**, 6584.

12 C. Bartual-Murgui, A. Cerf, C. Thibault, C. Vieu, L. Salmon, G. Molnár and A. Bousseksou, *Microelectron. Eng.*, 2013, **111**, 365.

13 I. A. Gural'skiy, C. M. Quintero, G. Molnár, I. O. Fritsky, L. Salmon and A. Bousseksou, *Chem. - A Eur. J.*, 2012, **18**, 9946.

14 I. A. Gural'skiy, G. Molnár, I. O. Fritsky, L. Salmon and A. Bousseksou, *Polyhedron*, 2012, **38**, 245.

15 J. Dugay, M. Giménez-Marqués, T. Kozlova, H. W. Zandbergen, E. Coronado and H. S. J. van der Zant, *Adv. Mater.*, 2015, **27**, 1288.

16 A. Rotaru, J. Dugay, R. P. Tan, I. A. Guralskiy, L. Salmon, P. Demont, J. Carrey, G. Molnár, M. Respaud and A. Bousseksou, *Adv. Mater.*, 2013, **25**, 1745.

17 A. Rotaru, I. a. Gural'skiy, G. Molnár, L. Salmon, P. Demont and A. Bousseksou, *Chem. Commun.*, 2012, **48**, 4163.

18 F. Prins, M. Monrabal-Capilla, E. A. Osorio, E. Coronado and H. S. J. Van Der Zant, *Adv. Mater.*, 2011, **23**, 1545.

19 A. Holovchenko, J. Dugay, M. Giménez-Marqués, R. Torres-Cavanillas, E. Coronado and H. S. J. van der Zant, *Adv. Mater.*, 2016, **28**, 7228.

20 J. Dugay, M. Aarts, M. Giménez-Marqués, T. Kozlova, H. W. Zandbergen, E. Coronado and H. S. J. Van Der Zant, *Nano Lett.*, 2017, **17**, 186.

21 C. Lefter, R. Tan, J. Dugay, S. Tricard, G. Molnár, L. Salmon, J. Carrey, A. Rotaru and A. Bousseksou, *Phys. Chem. Chem. Phys.*, 2015, **17**, 5151.

22 C. Lefter, R. Tan, S. Tricard, J. Dugay, G. Molnár, L. Salmon, J. Carrey, A. Rotaru and A. Bousseksou, *Polyhedron*, 2015, **102**, 434.

23 C. Lefter, R. Tan, J. Dugay, S. Tricard, G. Molnár, L. Salmon, J. Carrey, W. Nicolazzi, A. Rotaru and A. Bousseksou, *Chem. Phys. Lett.*, 2016, **644**, 138.

24 M. P. Pileni, *Adv. Colloid Interface Sci.*, 1993, **46**, 139.

25 Y. Raza, F. Volatron, S. Moldovan, O. Ersen, V. Huc, C. Martini, F. Brisset, A. Gloter, O. Stéphan, A. Bousseksou, L. Catala and T. Mallah, *Chem. Commun.*, 2011, **47**, 11501.

26 S. Titos-Padilla, J. M. Herrera, X.-W. Chen, J. J. Delgado and E. Colacio, *Angew. Chem.*, 2011, **123**, 3348.

27 J. M. Herrera, S. Titos-Padilla, S. J. a. Pope, I. Berlanga, F. Zamora, J. J. Delgado, K. V. Kamenev, X. Wang, A. Prescimone, E. K. Brechin and E. Colacio, *J. Mater. Chem. C*, 2015, **3**, 7819.

28 Y. a. Tobon, C. Etrillard, O. Nguyen, J.-F. Létard, V. Faramarzi, J.-F. Dayen, B. Doudin, D. M. Bassani and F. Guillaume, *Eur. J. Inorg. Chem.*, 2012, **2012**, 5837.

29 L. Moulet, N. Daro, S. Mornet, N. Vilar-Vidal, G. Chastanet and P. Guionneau, *Chem. Commun.*, 2016, **52**, 13213.

30 D. Qiu, L. Gu, X.-L. Sun, D.-H. Ren, Z.-G. Gu and Z. Li, *RSC Adv.*, 2014, **4**, 61313.

31 L. Moulet, N. Daro, C. Etrillard, J.-F. Létard, A. Grosjean and P. Guionneau, *Magnetochemistry*, 2016, **2**, 10.

32 A. Grosjean, N. Daro, B. Kauffmann, A. Kaiba, J.-F. Létard and P. Guionneau, *Chem. Commun.*, 2011, **47**, 12382.

33 A. Urakawa, W. Van Beek, M. Monrabal-Capilla, J. R. Galán-Mascarós, L. Palin and M. Milanesio, *J. Phys. Chem. C*, 2011, **115**, 1323.